Cell Reports, Volume *42*

Supplemental information

Anillin forms linear structures and facilitates furrow ingression after septin and formin depletion

Mikhail Lebedev, Fung-Yi Chan, Anna Lochner, Jennifer Bellessem, Daniel S. Osório, Elisabeth Rackles, Tamara Mikeladze-Dvali, Ana Xavier Carvalho, and Esther Zanin

Table S1: dsRNA generation, T7 sequence is underlined

Gene	Oligonucleotide 1	Oligonucleotide 2	Source	RNAi condition	Concentration [µg/µl]
cyk-1	TAATACGACTCACTATAGGTTGGAGTTCGATGCAGAAGA	TAATACGACTCACTATAGGTTGCCTTGTCAGGAACTGAA	cDNA	injection	0.5-1.0
nmy-2	TAATACGACTCACTATAGGAATTGAATCTCGGTTGAAGGAA	TAATACGACTCACTATAGGACTGCATTTCACGCATCTTATG	cDNA	injection	0.18-0.36
ani-1	TAATACGACTCACTATAGGAGCCGGAGTTGGAAAGCTG	TAATACGACTCACTATAGGCCTATTCTTTTCCAAACGTTGC	genomic DNA	injection	0.35-0.7
unc-61	TAATACGACTCACTATAGGAGCGTGTTAATGTGATCCCAG	TAATACGACTCACTATAGGTCCAGTCTCTCCATCTCCAATC	genomic DNA	injection	0.3-1.0
unc-59	TAATACGACTCACTATAGGTGGGAGCCAATAGTGAACTAC	TAATACGACTCACTATAGGCGATTCTTCTCATTCTTCGGC	genomic DNA	injection	0.3
arx-2	TAATACGACTCACTATAGGCAGCTTCGTCAAATGCTTG	TAATACGACTCACTATAGGTATTTCCATGCAATACGCG	cDNA	injection	1.0
perm-1	TAATACGACTCACTATAGGAATTTTCTAGGTCGTCAATCTTCA	TAATACGACTCACTATAGGCGAAAACGCGATCATTTTTA	genomic DNA	injection	0.1
perm-1	AATGTTTATGAACCCGAGCG	TTCACGCAGTTGTTGACACA	[1]	feeding	N.A.
ani-1	CATGTTCACTGACAACTGGGATA	CAAACTCAATGGAGAGGACAATC	Bioscience	feeding	N.A.

Supplemental FIGURE 1

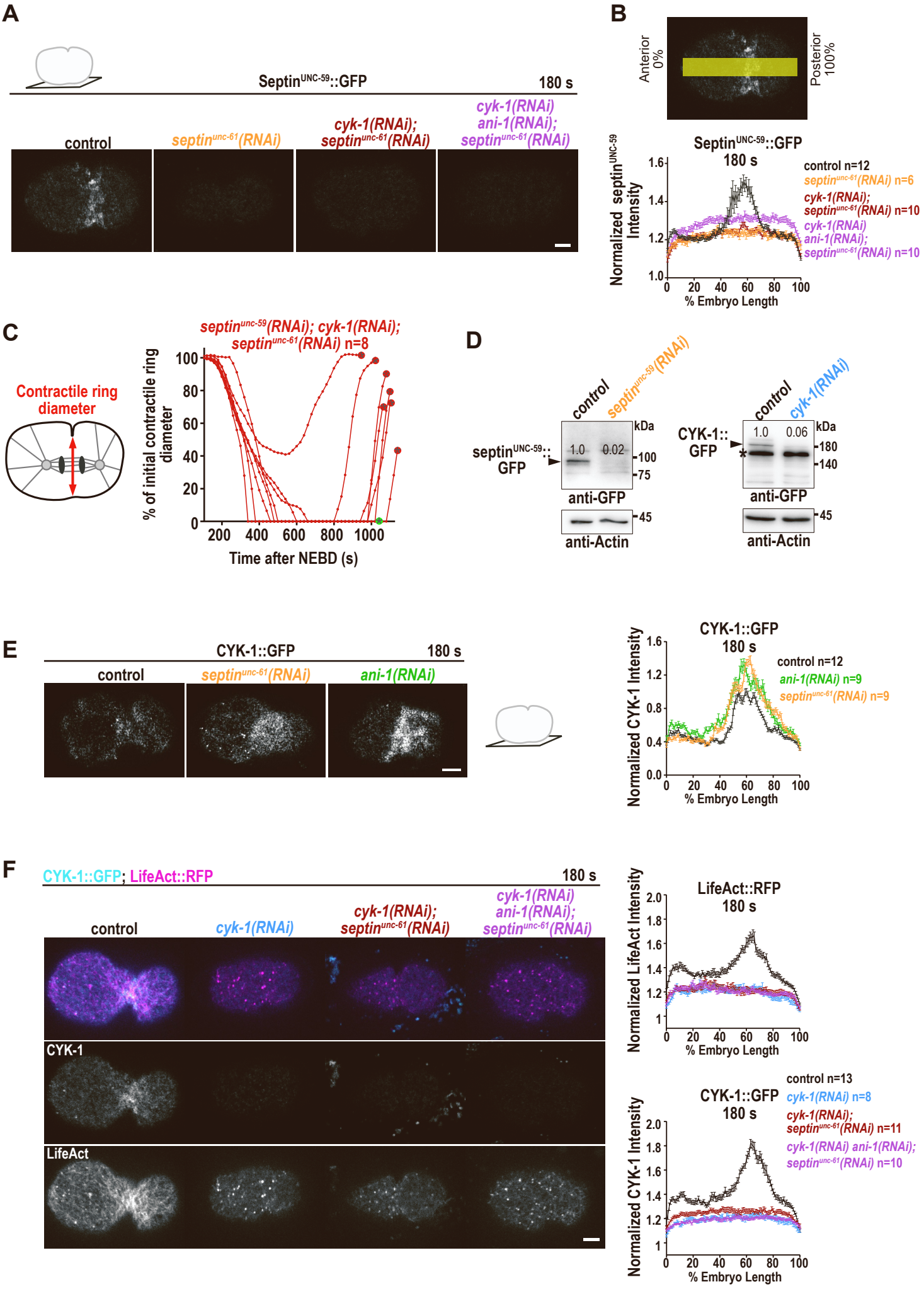

Figure S1 Single, double and triple RNAi co-depletions of CYK-1 and septin are highly efficient, related to Figure 1

A) Confocal single z-plane cortical images of endogenously tagged septin^{UNC-59}::GFP for indicated RNAi conditions 180 s after NEBD.

B) Normalized mean septin^{UNC-59}::GFP fluorescence intensity from the anterior (0% embryonic length) to the posterior (100%) cortex 180 s after NEBD for the indicated RNAi conditions.

C) The contractile ring diameter is plotted as % of the initial contractile ring diameter over time for individual embryos treated with *septin^{unc-59}(RNAi); cyk-1(RNAi); septin^{unc-61}(RNAi)*. Green and red encircled stars indicate whether embryos succeed or fail cytokinesis, respectively.

D) Immunoblot of septin^{UNC-59}::GFP and CYK-1::GFP expressing worms with and without *septin^{unc-59}(RNAi)* or *cyk-1(RNAi)* probed with antibodies against GFP and actin, as a loading control. The mean septin^{UNC-59}::GFP or CYK-1::GFP protein levels (3 worm extracts) are indicated, star indicates a non-specific band.

E) Confocal cortical single z-plane images of endogenously tagged CYK-1::GFP (left) and normalized mean CYK-1::GFP fluorescence intensity from the anterior to the posterior cortex 180 s after NEBD for indicated RNAi conditions (right).

F) Confocal cortical single z-plane images of endogenously tagged CYK-1::GFP (cyan) and LifeAct::RFP (magenta) expressing embryos for the indicated RNAi conditions 180 s after NEBD (left). Normalized mean CYK-1::GFP and LifeAct::RFP fluorescence intensity from the anterior to the posterior cortex 180 s after NEBD (right).

All scale bars are 5 µm, error bars are SEM and n=number of embryos analyzed.

Supplemental FIGURE 2

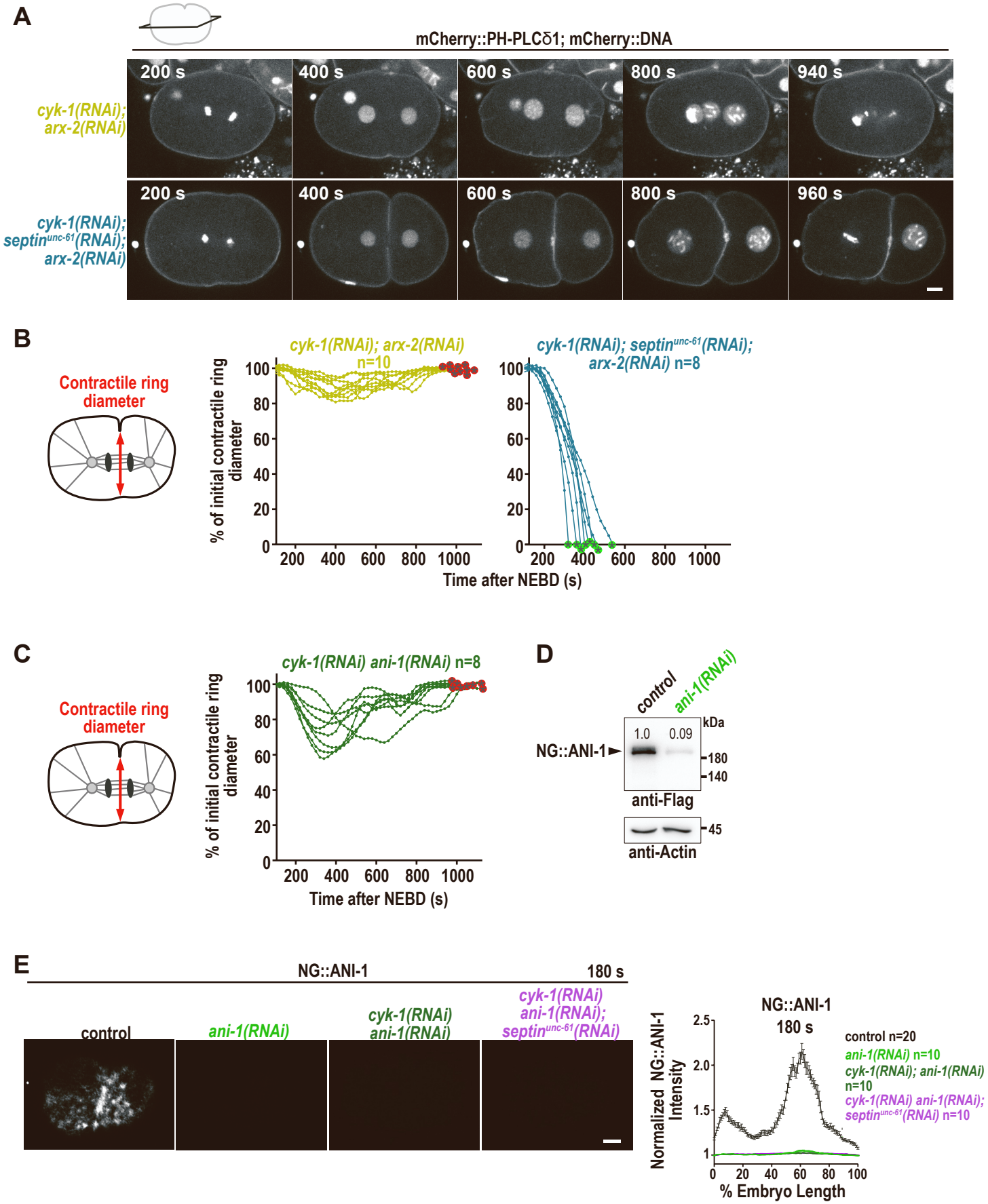

Figure S2 ARX-2 depletion does not prevent furrow ingression in *cyk-1(RNAi); septin^{unc-61}(RNAi)* embryos, related to Figure 1

A) Central plane images of embryos expressing the membrane marker mCherry::PH-PLCδ1 and mCherry::DNA (Histone-H2B) and treated with the indicated RNAi conditions.

B, C) The contractile ring diameter is plotted as % of the initial contractile ring diameter over time for individual embryos for indicated RNAi conditions. Green and red encircled stars indicate whether embryos succeed or fail cytokinesis, respectively.

D) Immunoblot of endogenously tagged NeonGreen::ANI-1 (NG::ANI-1) expressing worms with and without *ani-1(RNAi)* probed with antibodies against Flag and actin, as a loading control. The mean NG::ANI-1 protein levels (3 worm extracts) are indicated.

E) Confocal cortical single z-plane images of NG::ANI-1 (left) and normalized mean NG::ANI-1 fluorescence intensity from the anterior to the posterior cortex 180 s after NEBD for indicated RNAi conditions (right).

All scale bars are 5 µm, error bars are SEM and n=number of embryos analyzed.

Supplemental FIGURE 3

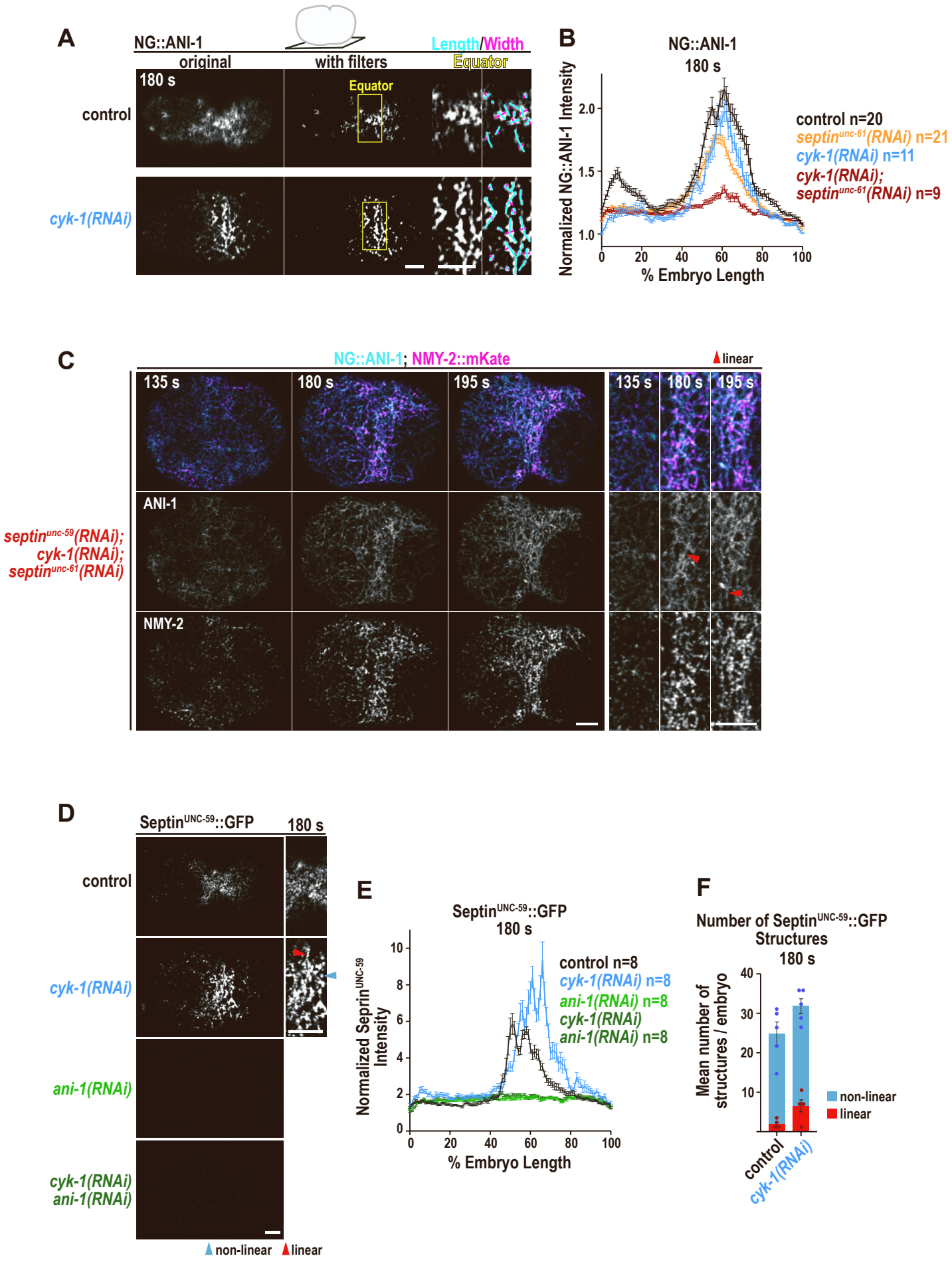

Figure S3 Equatorial septin^{UNC-59}::GFP levels are elevated after CYK-1 depletion and strongly reduced after ANI-1 depletion, related to Figure 2

A) After filtering the original image, the length and width of each structure was measured in a region at the cell equator unless stated otherwise. Structures with a length/with ratio ≥4 were classified as linear and a length/with ratio <4 as non-linear.

B) Mean normalized NG::ANI-1 fluorescence intensity from the anterior to the posterior cortex at 180 s after NEBD for indicated RNAi conditions. The control NG::ANI-1 graph is reproduced from Fig. S2E.

C) Confocal single z-plane images of the cell cortex of endogenously tagged NG::ANI-1 (cyan) and NMY-2::mKate (magenta) for *septin^{unc-59}(RNAi); cyk-1(RNAi); septin^{unc-61}(RNAi)* embryos. Magnification of the equatorial region of the same embryos are shown on the right.

D) Confocal single z-plane images and magnifications of the equatorial region of embryos with endogenously GFP-tagged septin^{UNC-59} at 180 s after NEBD are shown.

E) Mean normalized septin^{UNC-59}::GFP fluorescence intensity from the anterior to the posterior cortex for indicated RNAi conditions at 180 s after NEBD.

F) Mean number of septin^{UNC-59}::GFP structures per embryo for the indicated conditions at 180 s after NEBD. Dots represent data points of individual embryos.

Linear structures are highlighted by red and non-linear by blue arrowheads. Error bars are SEM, all scale bars are 5 µm, n=number of embryos analyzed.

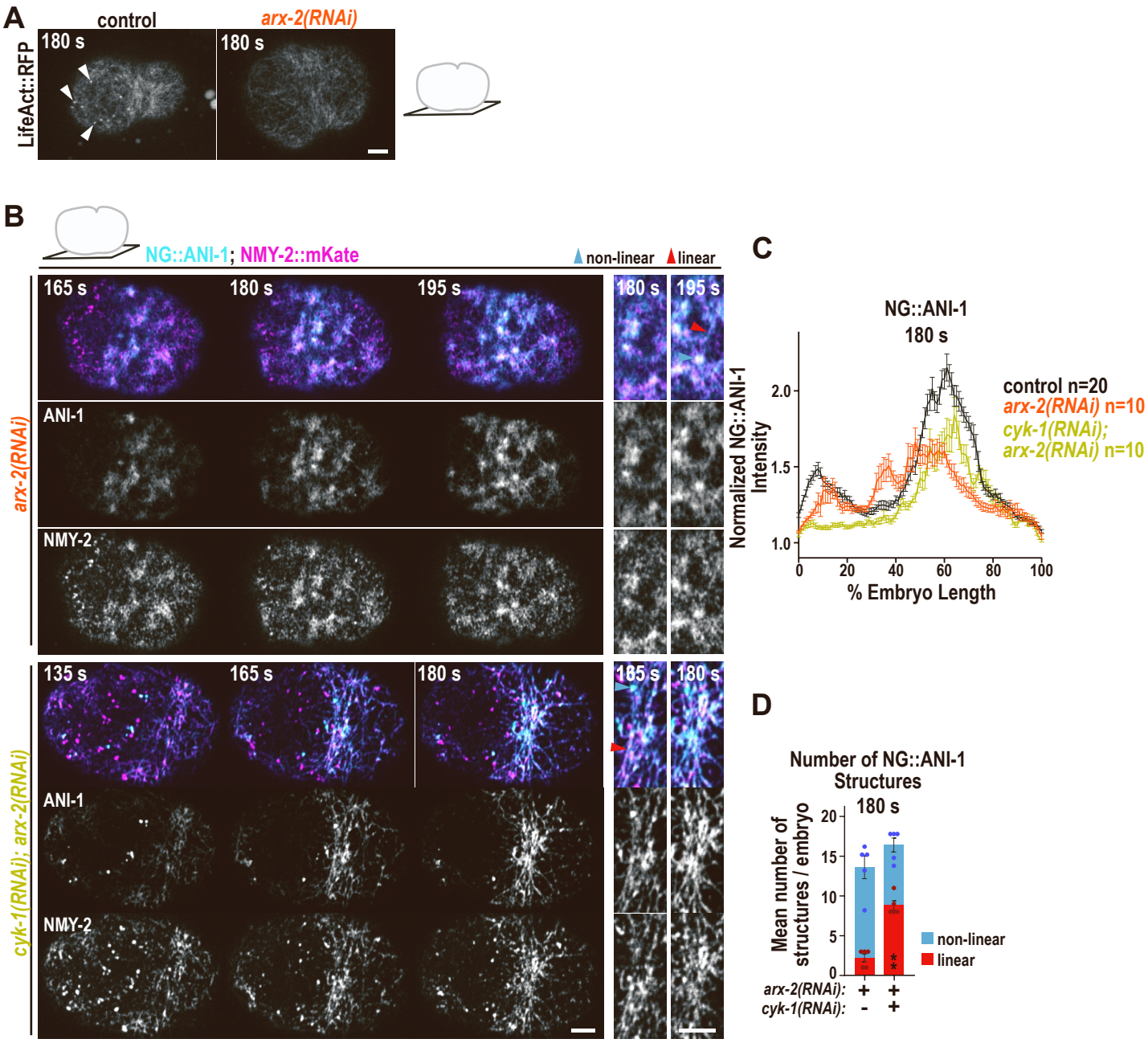

Figure S4 ARX-2 depletion does not influence NG::ANI-1 localization, related to Figure 2

A) Confocal single z-plane images of LifeAct::RFP for control and *arx-2(RNAi)* embryos at 180 s after NEBD. After *arx-2(RNAi)* F-actin puncta (white arrowheads) disappear.

B) Confocal single z-plane images of the cell cortex of NG::ANI-1 (cyan) and NMY-2::mKate (magenta) after *arx-2(RNAi)* or *cyk-1(RNAi); arx-2(RNAi)*. Magnification of the cell equator is shown on the right. Note: cleavage furrow ingression is delayed in *arx-2(RNAi)* in comparison to control embryos (compare with Fig. 2A, 180 s). Linear structures are highlighted by red and non-linear by blue arrowheads.

C) Normalized mean NG::ANI-1 fluorescence intensity from the anterior to the posterior cortex at 180 s after NEBD for indicated RNAi conditions. Control graph is reproduced from Fig. S2E and n=number of embryos analyzed.

D) The mean number of linear and non-linear NG::ANI-1 structures per embryo at an equatorial region for the indicated RNAi conditions at 180 s after NEBD. P-value was calculated using Mann-Whitney-U test and represents ** p<0.01 in comparison to *arx-2(RNAi)* treated embryos and dots represent data points of individual embryos.

All scale bars are 5 µm and error bars are SEM.

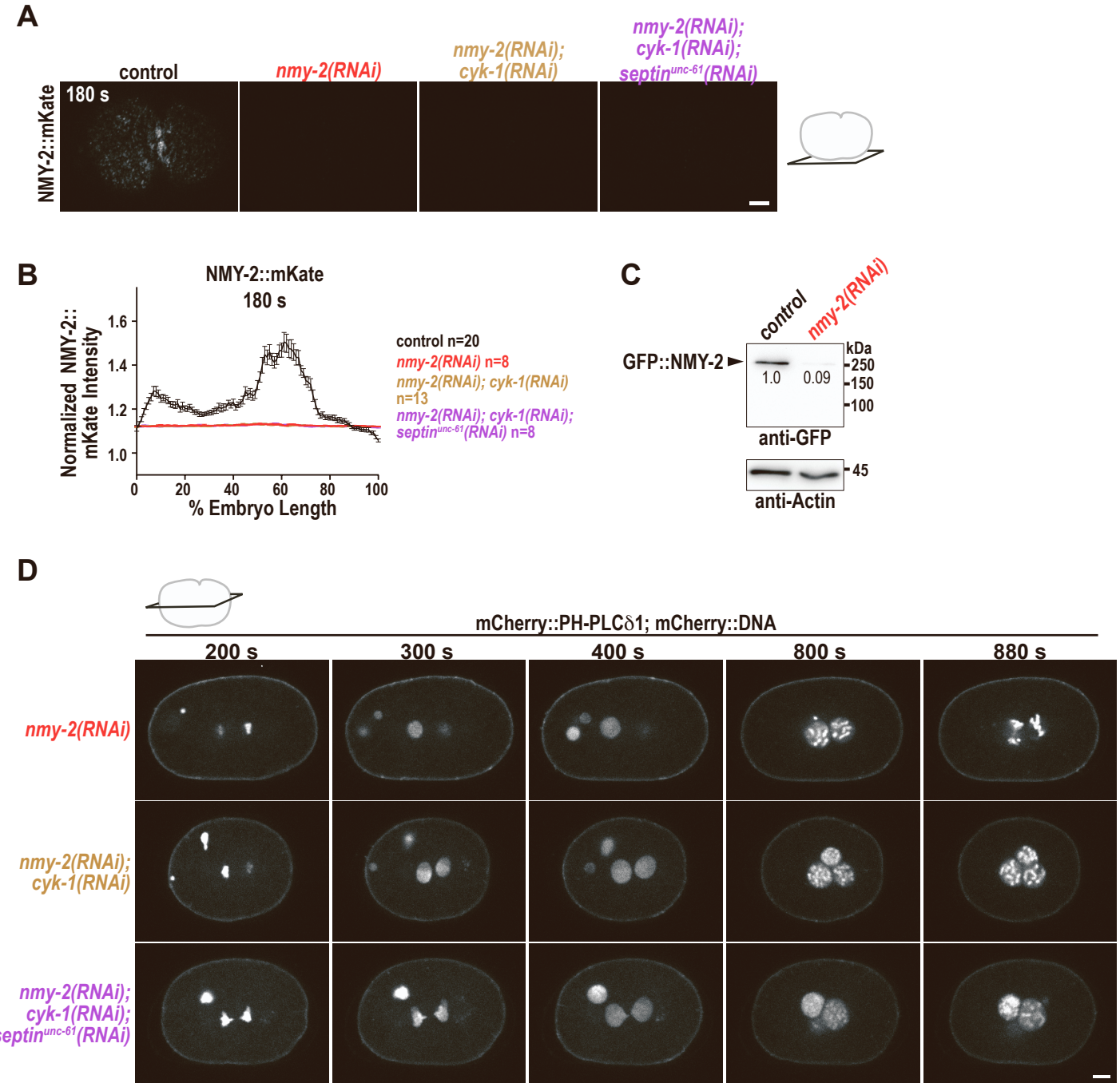

Figure S5 Single, double and triple RNAi co-depletions of NMY-2, CYK-1 and septin^{UNC-61} are highly efficient, related to Figure 3

A) Confocal single z-plane cortical images of NMY-2::mKate for indicated RNAi conditions 180 s after NEBD.

B) Graphs display the mean normalized NMY-2::mKate cortical fluorescence intensity for the indicated RNAi conditions 180 s after NEBD.

C) Immunoblots of adults worms expressing endogenously-tagged GFP::NMY-2 with or without *nmy-2(RNAi)* and probed with the indicated antibodies. The mean intensity of the GFP::NMY-2 band is shown (3 worm extracts).

D) Central plane images of embryos expressing the general membrane marker mCherry::PH-PLC1 and mCherry::DNA (Histone-H2B) and treated with the indicated RNAi conditions and time points after NEBD.

E) Normalized cortical NG::ANI-1 fluorescence intensity for indicated RNAi conditions 180 s after NEBD. Control graph reproduced from Fig. S2E.

Error bars are SEM, scale bars are 5 μm and n= number of embryos analyzed.

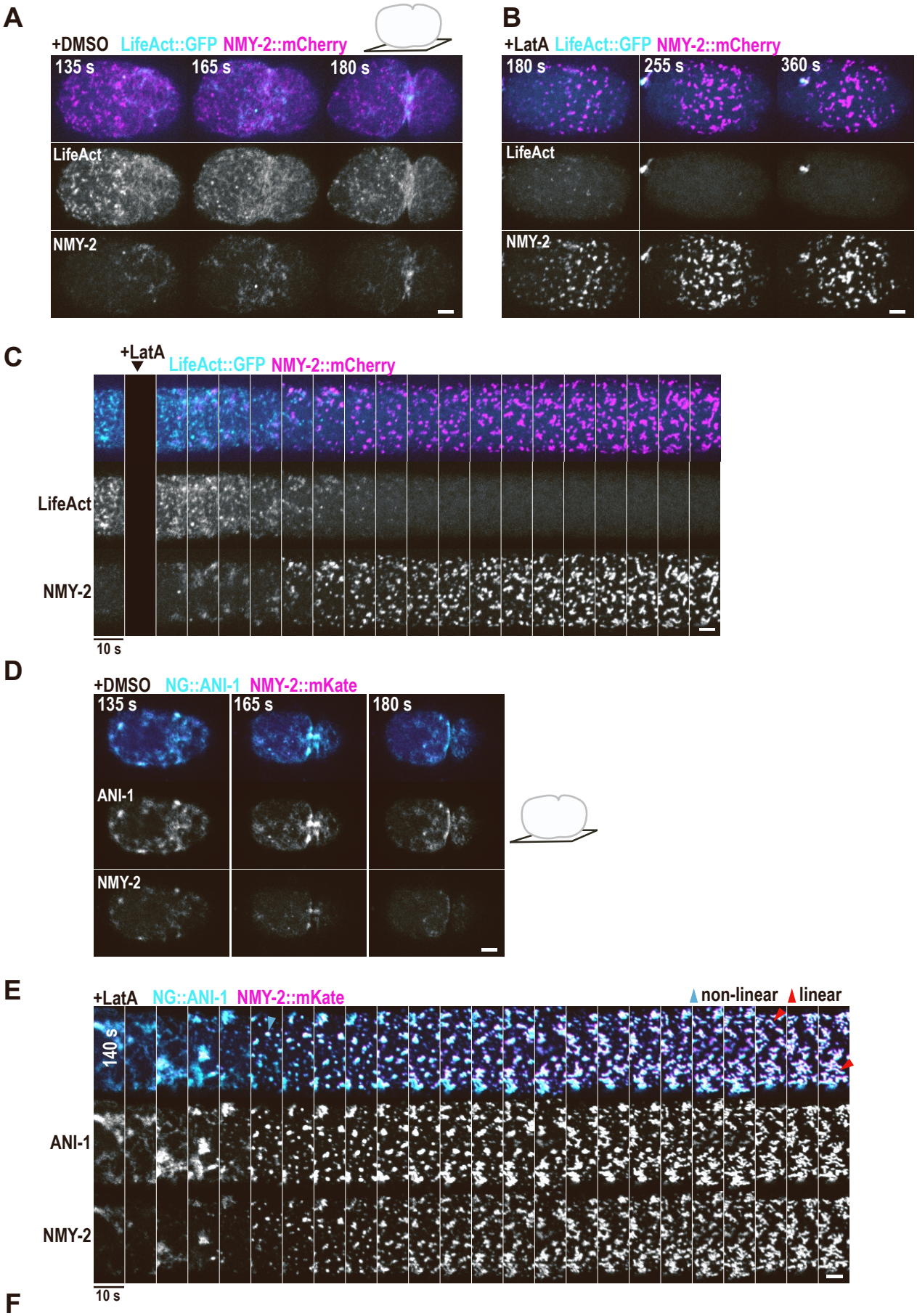
A
+DMSO LifeAct::GFP NMY-2::mCherry
135 s
165 s
180 s
LifeAct
NMY-2
B
+LatA LifeAct::GFP NMY-2::mCherry
180 s
255 s
360 s
LifeAct
NMY-2
C
+LatA
LifeAct::GFP NMY-2::mCherry
LifeAct
NMY-2
10 s
D
+DMSO NG::ANI-1 NMY-2::mKate
135 s
165 s
180 s
ANI-1
NMY-2
E
+LatA NG::ANI-1 NMY-2::mKate
non-linear
linear
140 s
ANI-1
NMY-2
10 s
F
NG::ANI-1
NMY-2::mKate
Normalized ANI-1 Intensity
Normalized NMY-2 Intensity
% Embryo Length
control n=10 (165 s)
+LatA n=8 (165 s)
+LatA n=8 (255 s)

Figure S6 Cortical fluorescence intensities of NMY-2::mKate and NG::ANI-1 after Latrunculin A treatment, related to Figure 4

A-C) Maximum intensity projections of 10 cortical z-planes of permeabilized one-cell embryos expressing NMY-2::mCherry (magenta) and LifeAct::GFP (cyan) treated with DMSO (A) or Latrunculin A (B, C). Panel (C) shows a kymograph of the equatorial region of the embryo in panel (B).

D, E) Maximum intensity projections of 10 cortical z-planes of permeabilized one-cell embryos expressing NMY-2::mKate (magenta) and NG::ANI-1 (cyan) treated with DMSO (D) or Latrunculin A (E). Panel (E) shows a kymograph of the equatorial region of the embryo of Fig. 4A.

F) Normalized mean cortical NMY-2::mKate and NG::ANI-1 fluorescence intensity from the anterior to the posterior cortex for control and Latrunculin A treated embryos at indicated time points.

Error bars are SEM, scale bars are 5 µm and n=number of embryos analyzed.

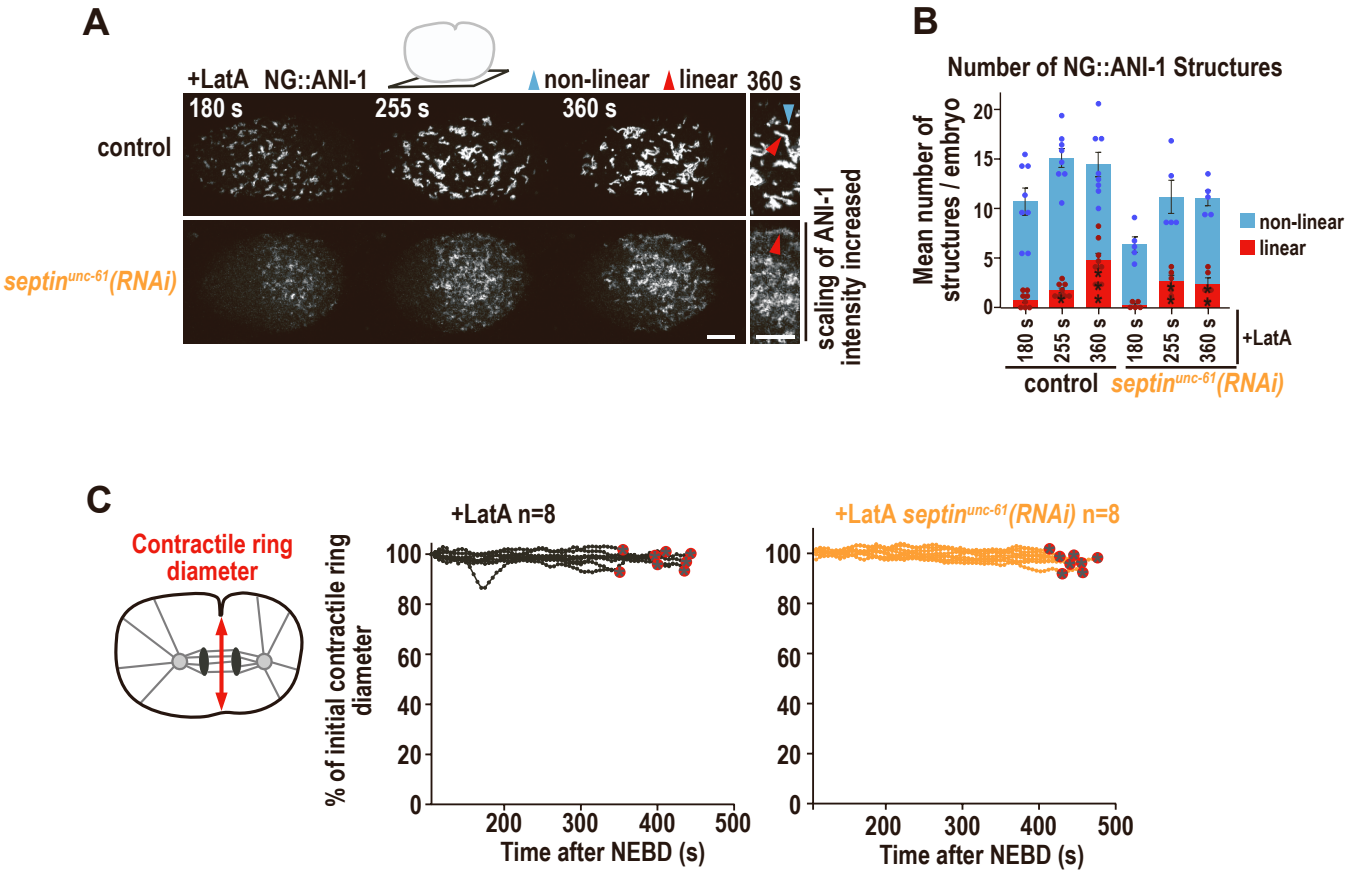

Figure S7 Septin^{UNC-61} facilitates linear structure formation in the absence of F-actin, related to Figure 4
A) Maximum intensity projections of 6 cortical z-planes of permeabilized one-cell embryos expressing NG::ANI-1 and treated without and with *septin^{unc-61}(RNAi)* and Latrunculin A. Intensity scaling of *septin^{unc-61}(RNAi)* embryo was increased.
B) Mean number of NG::ANI-1 structures at the cell equator per embryo without and with *septin^{unc-61}(RNAi)* and Latrunculin A treatment. Error bars are SEM, *P*-values were calculated using Mann-Whitney-U or student *t*-test and represent * p<0.05, ** p<0.01, *** p<0.001 in comparison to 180 s, dots represent data points of individual embryos. Control condition is reproduced from Fig. 4B.
C) Plotted is the contractile ring diameter of each embryo over time for Latrunculin A treated embryos with and without *septin^{unc-61}(RNAi)*, n=number of embryos analyzed. Red encircled stars indicate that embryos fail cytokinesis.

Supplemental FIGURE 8

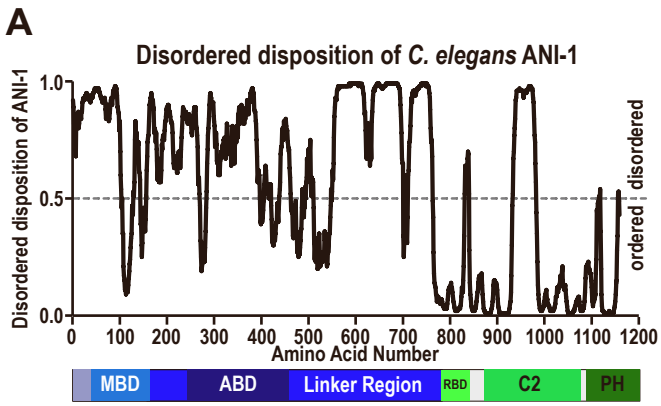

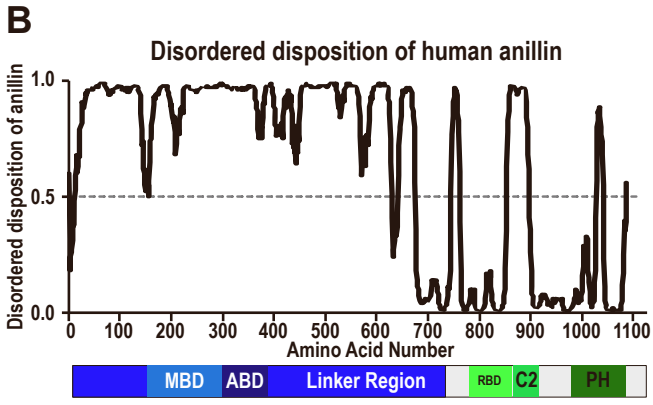

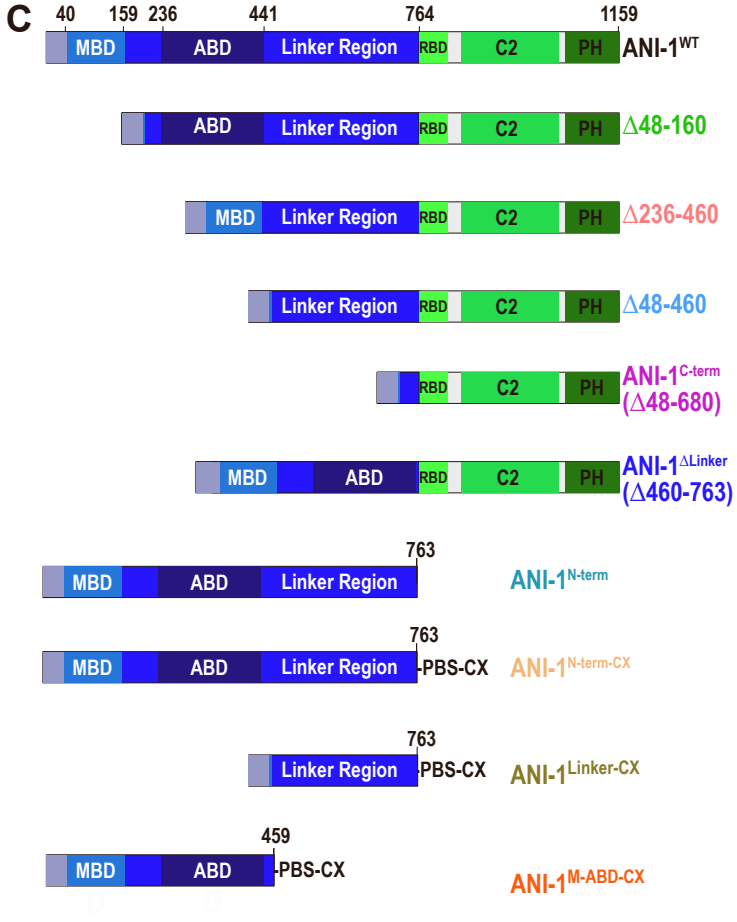

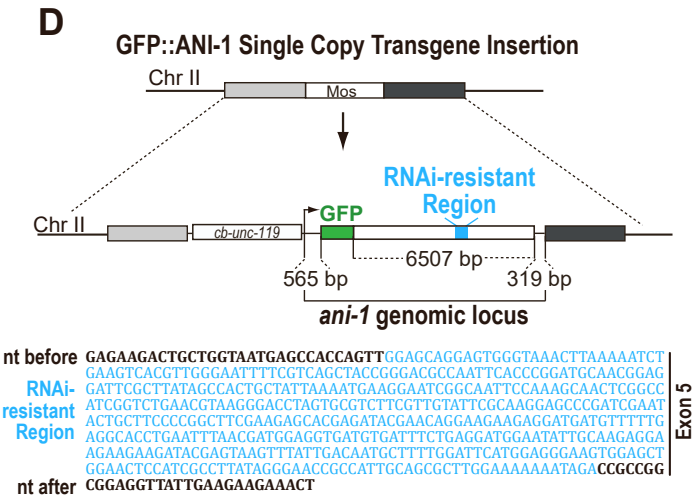

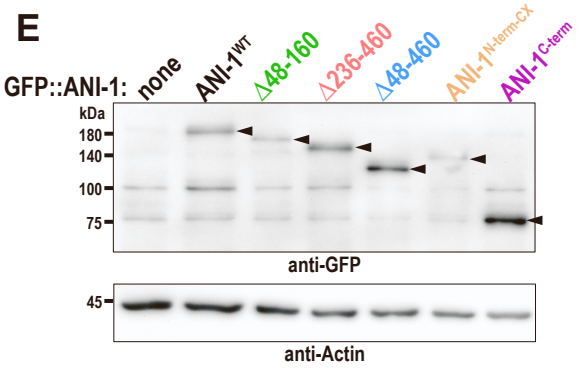

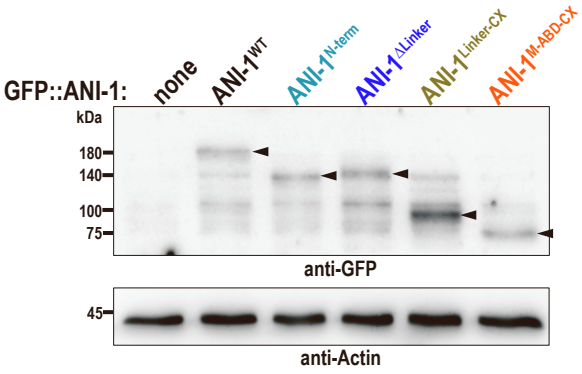

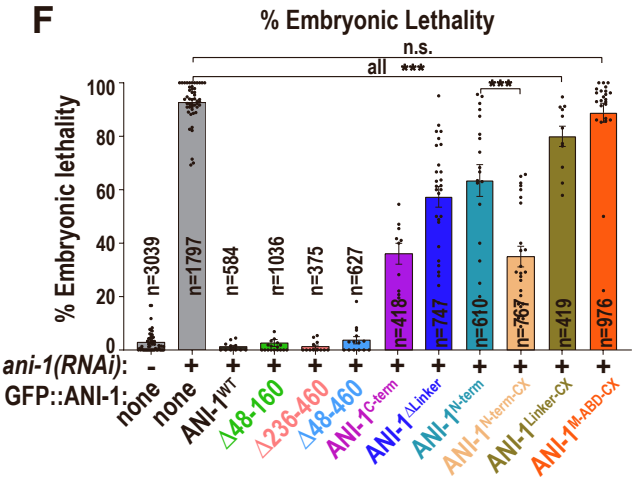

Figure S8 The N-terminal halves of *C. elegans* and human anillin are predicted to be highly disordered, related to Figure 5

A-B) Graphs display the predicted disordered regions of *C. elegans* ANI-1 and human anillin which were determine with DISOPRED3 [S2]. For comparison a scheme of their functional domains is shown below.

C) Schematic representation of GFP-tagged ANI-1^{WT} and tested ANI-1 mutant proteins.

D) GFP-tagged ANI-1 transgenes were integrated into the 'Mos' site on chromosome II. The ANI-1 transgenes comprise the genomic *ani-1* locus and *gfp*. Transgenes are resistant to *ani-1* RNAi targeting by re-encoding exon 5 but keeping the amino acid sequence and codon usage the same.

E) Immunoblots of adult worms expressing the indicated GFP-tagged ANI-1 proteins probed with anti-GFP and anti-actin antibodies.

F) Graph is plotting the mean percentage of embryonic lethality for the indicated GFP-tagged ANI-1 proteins and RNAi conditions. P-values were calculated using Mann-Whitney-U or student *t*-test and represent n.s. $p>0.05$ and *** $p<0.001$. Error bars are SEM and n= number of progeny (larvae and embryos) counted.

Supplemental FIGURE 9

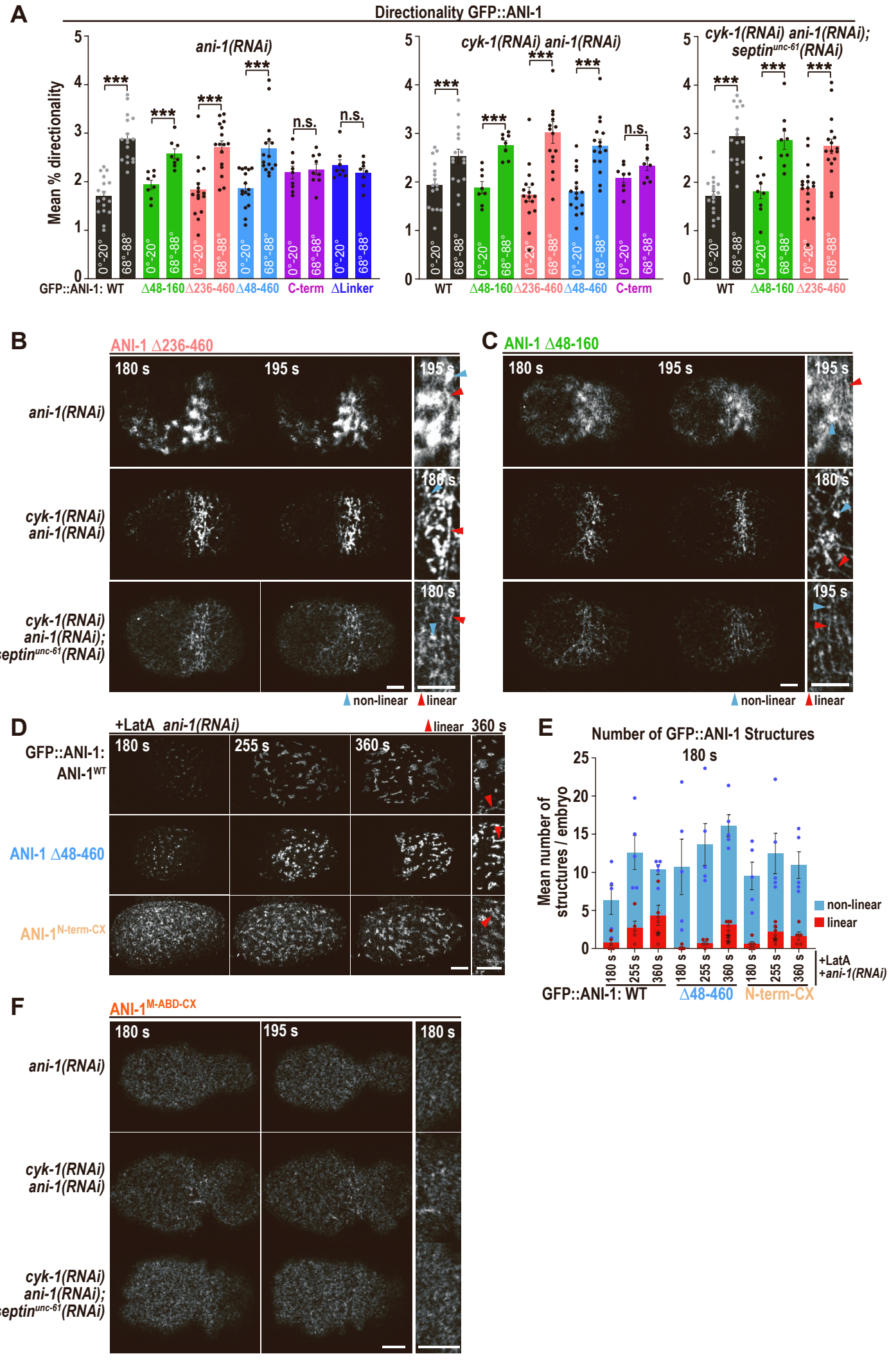

Figure S9 The MBD and ABD are not required for circumferential ANI-1 alignment, related to Figure 5

A) Mean percentage of 0-20º (anterior to posterior) and 68-88º (circumferentially) directionality measured for GFP-tagged ANI-1 proteins for indicated RNAi conditions 180 s after NEBD. *P*-values were determined with student *t*-test and represent *** $p<0.001$ and n.s. $p>0.05$.

B, C) Confocal cortical single z-plane images of GFP-tagged ANI-1 ∆236-460 (B) and ANI-1 ∆48-160 (C) expressing embryos for the indicated RNAi conditions and time points after NEBD. To better visualize the localization of GFP- tagged ANI-1 after septin^{UNC-61} co-depletion, the signal intensity scaling was increased in those conditions.

D) Maximum intensity projections of 6 cortical z-planes of permeabilized one-cell embryos expressing indicated GFP::ANI-1 transgenes and treated with Latrunculin A and *ani-1(RNAi).* Intensity scaling of ANI-1$^{N-term-CX}$ was increased.

E) Mean number of structures for indicated GFP::ANI-1 transgenes at the cell equator per embryo after *ani-1(RNAi)* and Latrunculin A treatment. *P*-values were calculated using Mann-Whitney-U or student *t*-test and represent * $p<0.05$, ** $p<0.01$ in comparison to 180 s.

F) Confocal cortical single z-plane images of GFP-tagged ANI-1$^{M-ABD-CX}$ expressing embryos for the indicated RNAi conditions and time points after NEBD.

For all cortical images: magnification of equatorial regions are shown on the right. Linear structures are highlighted by red and non-linear by blue arrowheads. Error bars are SEM and dots represent data points of individual embryos. Scale bars are 5 µm.

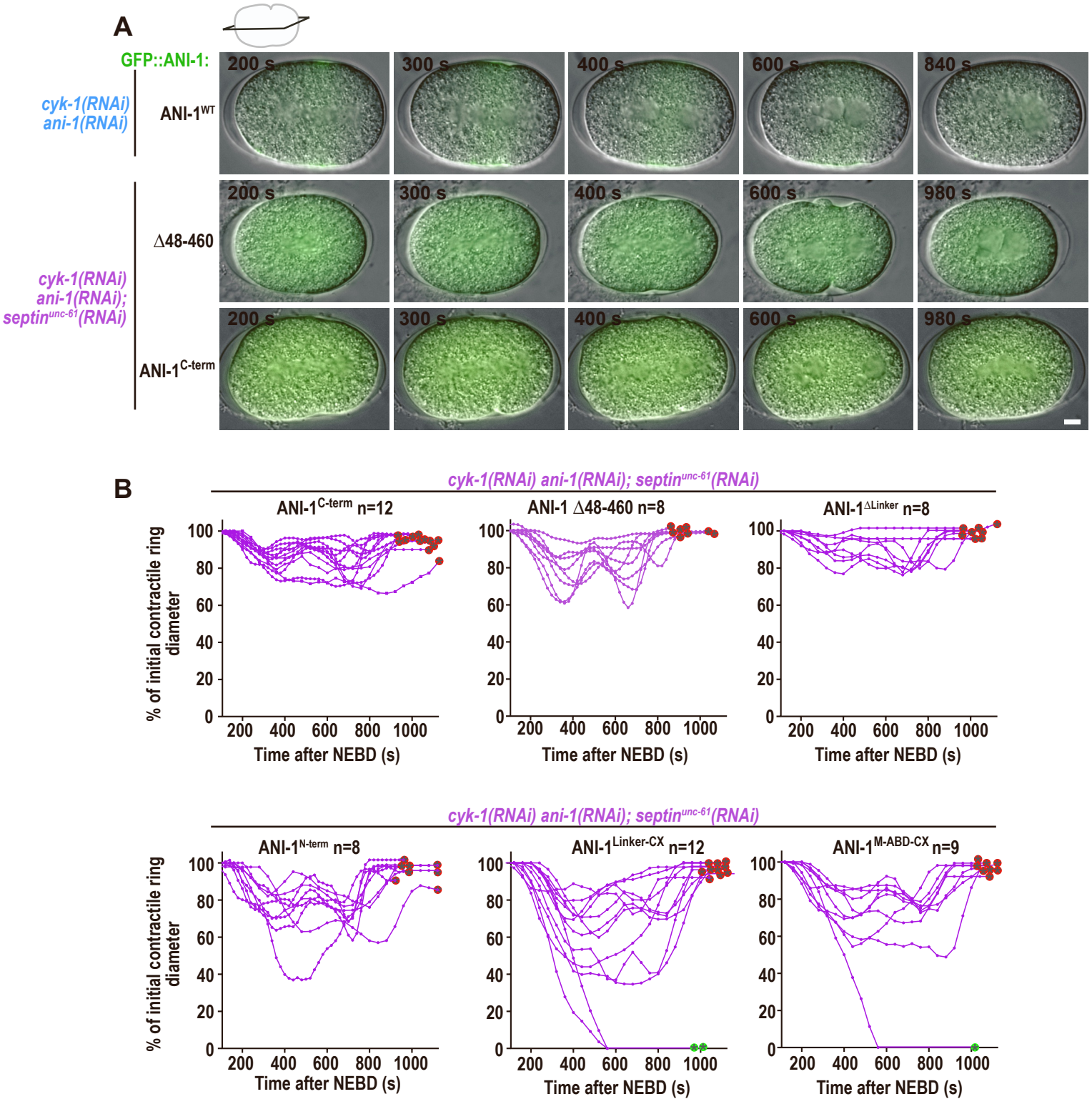

Figure S10 The Δ48-460 ANI-1 and ANI-1$^{C\text{-}term}$ mutants do not support furrow ingression after co-depletion of septins and formin, related to Figure 7

A) Merged central plane DIC and wide-field fluorescent images of the GFP-tagged ANI-1^{WT}, ANI-1$^{C\text{-}term}$ and ANI-1 Δ48-460 proteins for the indicated RNAi conditions and time points after NEBD. Scale bar is 5 μm.

B) Plotted is the contractile ring diameter of each embryo over time for indicated GFP-tagged ANI-1 mutant proteins and RNAi conditions, n=number of embryos analyzed. Green and red encircled stars indicate whether embryos succeed or fail cytokinesis, respectively.

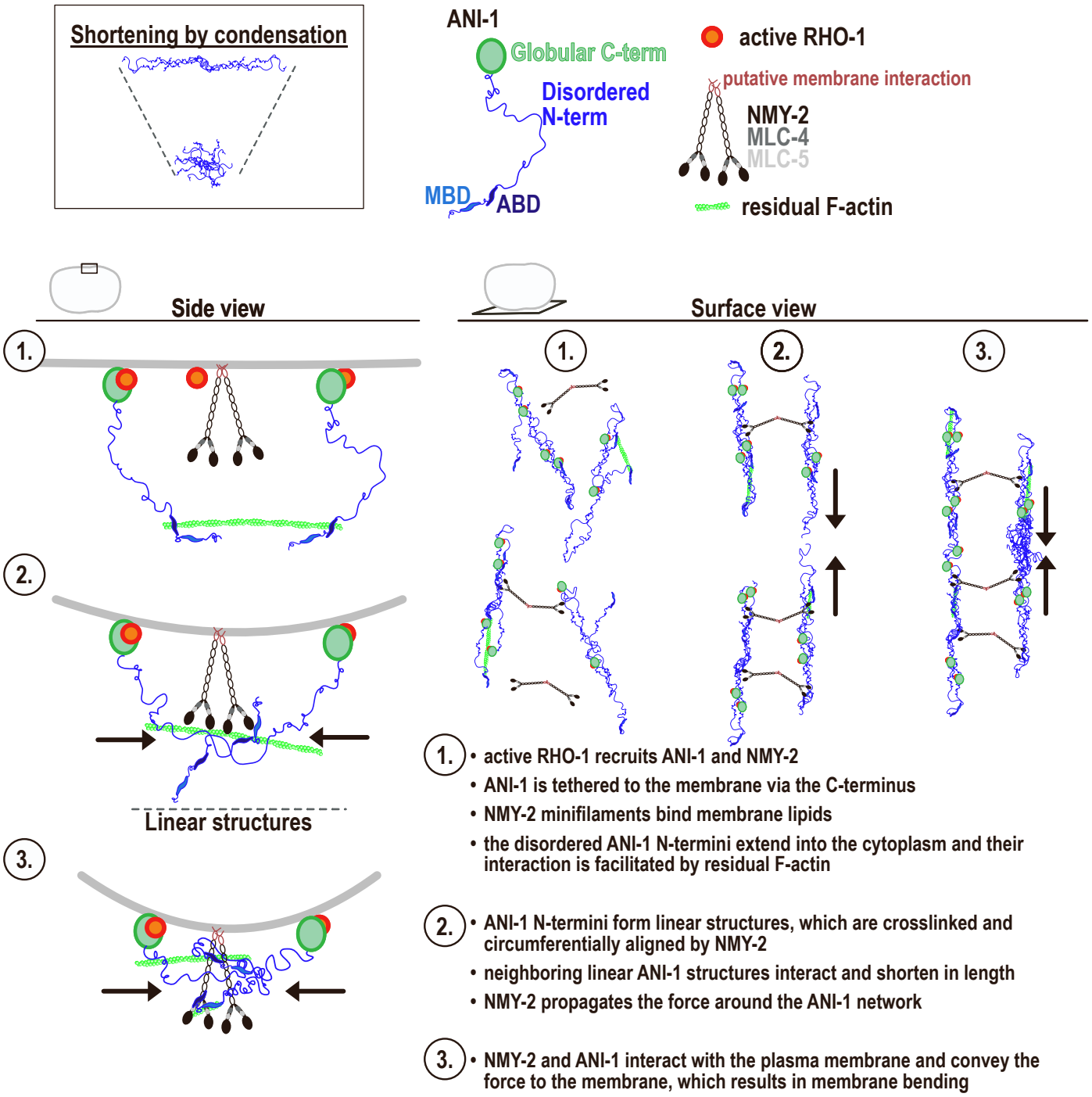

Figure S11, related to Discussion
Model illustrating how contraction of the ANI-1 network mediates cleavage furrow formation and ingression after the depletion of septins and formin.

Supplemental References:

[S1] Carvalho, A., S.K. Olson, E. Gutierrez, K. Zhang, L.B. Noble, E. Zanin, A. Desai, A. Groisman, and K. Oegema. 2011. Acute Drug Treatment in the Early *C. elegans* Embryo. PLoS ONE. 6:e24656-24658.

[S2] Jones, D.T., and D. Cozzetto. 2015. DISOPRED3: precise disordered region predictions with annotated protein-binding activity. Bioinformatics (Oxford, England). 31:857-863.